

Carbon Dioxide Corrosion in Wet Gas Annular Flow at Elevated Temperature

Y. Sun,^{†*} T. Hong,^{**} and C. Bosch^{***}

ABSTRACT

Wet gas corrosion rates of plain carbon steel at the top and bottom of a high-pressure, 10-cm-diameter, horizontal pipeline were measured under annular flow conditions at 0.45 MPa carbon dioxide (CO₂) and 90°C. The corrosive medium consisted of deionized water and a low viscosity hydrocarbon phase at water cuts of 80%. Superficial gas velocities (V_{sg}) of 15 m/s and 20 m/s were applied at a superficial liquid velocity (V_{sl}) of 0.05 m/s for 100 h. The corrosion rates measured by electrical resistance (ER) technique advanced in three stages, showing an exponential decay corresponding to the iron carbonate (FeCO₃) scale forming process. The general corrosion rates measured by ER were low, which were also confirmed by the coupon weight-loss measurements of average corrosion rates. No flow-induced localized corrosion (FILC) was found for the flow and corrosion conditions applied. Surface analysis techniques such as scanning electron microscopy (SEM) and x-ray photoelectron spectroscopy (XPS) revealed that the FeCO₃ film forming process was flow dependent and different for scales formed on the top and on the bottom of the pipe, resulting in different crystal sizes. Cross-sectional analysis by use of metallurgical microscope

(MM) indicates that a low thickness of the corrosion product film, usually <10 μm, was responsible for the high protection of the scales formed under these conditions.

KEY WORDS: annular flow, carbon dioxide corrosion, carbon steel, corrosion rate, iron carbonate film, localized attack, surface analysis, wet gas

INTRODUCTION

In the natural gas industry, conventional production facilities involve the removal of liquid and transportation of dry gas. This avoids problems with liquid holdup, slugging, hydrates, and corrosion.¹ As off-shore processing is costly, multiphase transportation of oil/water/gas mixtures over long distance transportation lines is now a common feature in offshore production systems. Multiphase flow is known to result in significant internal corrosion problems for carbon steel pipelines.² Dissolved carbon dioxide (CO₂) in the liquid phase of formation water or stemming from condensed moisture as a result of the reduction in temperature and pressure along the length of the pipe forms weak carbonic acid (H₂CO₃), which acts as the primary initiator to corrosion for carbon steel pipelines.³

Corrosion in horizontal pipelines is generally expected to be most severe at the bottom of the pipeline, particularly under slug flow conditions. However, in wet gas pipelines, top-of-the-line corrosion (TLC) can also take place because the fresh condensing water is very corrosive.⁴ On the other hand, the typical flow patterns encountered in wet gas pipelines are stratified flow, annular flow, and annu-

Submitted for publication August 2002; in revised form, March 2003. Presented as paper no. 02281 at CORROSION/2002, April 2002, Denver, CO.

[†] Corresponding author.

* NSF I/UCRC, Corrosion in Multiphase Systems Center, Institute for Corrosion and Multiphase Technology, Ohio University, 300 W. State St., Athens, Ohio 45701. Present address: BP America Inc., 501 Westlake Park Blvd., WL1-18.122, Houston, TX 77079.

** NSF I/UCRC, Corrosion in Multiphase Systems Center, Institute for Corrosion and Multiphase Technology, Ohio University, 300 W. State St., Athens, Ohio 45701. Present address: Monsanto Chemical Co., 800 N. Lindbergh Blvd., St. Louis, MO.

*** Mannesmann Forschungsinstitut GmbH, PO Box 25 11 16, 47251 Duisburg, Germany.

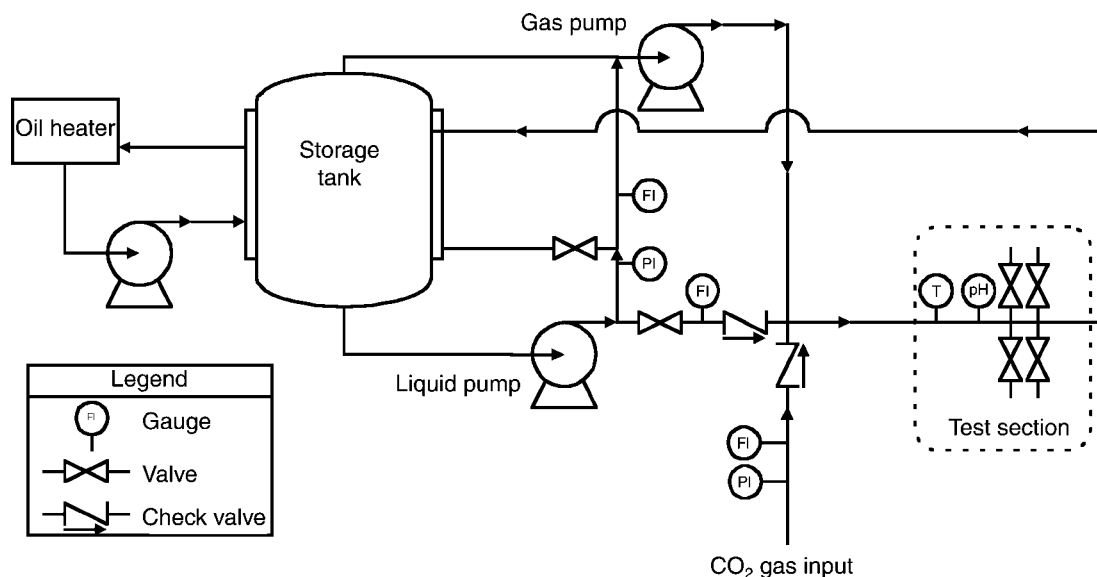


FIGURE 1. Schematic of the high-pressure inclinable flow loop system.

lar mist flow. These flow patterns also enhance internal corrosion along the top and bottom of a pipe.

Most work in understanding corrosion in oil and gas pipelines has been carried out with single-phase water or two-phase gas/water systems.⁵⁻¹⁰ Moreover, small scale laboratory tests such as the rotating cylinder electrode, jet impingement, bubble tests, and small diameter flow loops are suitable methods for studying flow effects on corrosion. These experimental systems provide easy and inexpensive testing under controlled conditions. However, these methods do not take into account the effect of multiphase flow and the presence of various flow regimes encountered in oil/water/gas pipelines. Hence, a scale-up of these results to multiphase flow under field conditions can lead to serious errors in the prediction of corrosion rates and flow-induced localized corrosion (FILC) under field conditions.

Apparently, knowledge about the formation of corrosion products by surface analysis should closely correspond to corrosion studies. The formation of corrosion products and their morphology strongly depends upon the flow regime, solution chemistry, geometry, pH, CO₂ partial pressure, and temperature.³ These parameters influence the corrosion mechanism and, therefore, the resulting corrosion rates. The corrosion products formed vary accordingly. A lot of research has been done in understanding the corrosion product film properties,^{5,8,10-12} but so far, no information is available on the flow-dependent change of properties of iron carbonate (FeCO₃) scales under multiphase wet gas corrosion conditions.

In practice, most pipeline failures are caused by localized corrosion instead of uniform corrosion, such as flow-independent pitting and/or FILC, often called erosion-corrosion. The initiation of FILC has been extensively studied by Schmitt and coworkers in theory as well as in high-pressure laboratory scale tests and large scale multiphase slug flow.¹³⁻¹⁷ However, no research about critical conditions for the initiation of FILC in wet gas conditions has been done so far.

EXPERIMENTAL PROCEDURES

Flow Loop and Test Section

A unique, 18-m-long, 10-cm-diameter, high-pressure, high-temperature, inclinable flow loop was used to study CO₂ wet gas corrosion (Figure 1). The entire loop is manufactured from Type 316 (UNS S31600)⁽¹⁾ stainless steel (SS). A predetermined oil/water mixture was stored in a 1.4-m³ tank, which served as a storage tank as well as a separation unit for the multiphase gas/oil/water mixture. The tank was heated by a heating jacket and two 3-kW immersion heaters. Heat transfer oil was preheated in a separate tank using four 3.7-kW heaters and pumped through the heating jacket of the storage tank. Liquid was moved through this system by a SS variable speed centrifugal pump. The flow was controlled within a range of 0 to 100 m³/h with the variable speed pump in conjunction with a recycle stream. The flow rate was controlled by an inline turbine meter.

A fresh gas feed line at 2 MPa pressure supplied CO₂ gas from a 20,000-kg storage tank. This line was initially used to pressurize the system and for calibration purposes when the system was running with once-through gas. In normal operation, gas is con-

⁽¹⁾ UNS numbers are listed in *Metals and Alloys in the Unified Numbering System*, published by the Society of Automotive Engineers (SAE International) and cosponsored by ASTM International.

tinuously circulated through the system at desired speeds by a multiphase progressing cavity pump, driven by a variable speed motor through a reduction gear system. An exhaust line with a knock out drum was used to vent gas from the system if required.

The test section was a 10-cm-diameter, 2-m-long schedule 80 SS pipe, as shown in Figure 2. The two pairs of ports at the top and at the bottom were used to insert flush-mountable ER probes and coupon holders for corrosion rate measurements. The pressure tappings were connected to pressure transducers and used for pressure drop measurements. The differential transducer taps were set up 7.0 m apart on the bottom of the pipe in the test section. Ports for insertion of a pH probe, the sampling tube, and the thermocouple were provided accordingly.

Specimen Preparation

In this study, circular coupons of hot-rolled plain carbon steel⁽²⁾ with a diameter of 11.6 mm and a thickness of 3.1 mm were used for weight-loss measurements. The chemical composition of the carbon steel is given in Table 1.

The coupon holder was designed for insertion of four flush-mounted coupons at the same time (Figure 3). Prior to testing, the coupons were polished by silicon carbide (SiC) paper up to 600 grit, then rinsed with distilled water, degreased with acetone (CH_3COCH_3), and air-dried. Finally, the coupons were weighed and immediately introduced into the system.

The post-test cleaning procedure was performed by rinsing the coupons with acetone to remove the hydrocarbon phase, drying, and then storing them for surface analysis. Afterward, the specimens were pickled in inhibited 10% hydrochloric acid (HCl) for removal of corrosion products, neutralized in alkali, rinsed with distilled water and acetone, air-dried, and weighed for mass-loss measurements.

Experimental Procedure

The test liquid consisted of deionized water and a refined oil with a density of 800 kg/m^3 and a viscosity of 2 cp at 40°C , which served as the hydrocarbon phase. The oil and water were mixed using a recycle line back to the upper level of the tank during the entire operation. The water cut in the pipe sent to the test section was also monitored by withdrawing samples of the test fluid. The flow rate of the recycle stream was then adjusted accordingly to achieve the desired fluid composition. The system eventually contained 315 gal (1.2 m^3) of test solution at 80% water cut. The system was then deoxygenated by once-through passing of CO_2 at a low constant rate for about 4 h to 5 h. The levels of dissolved oxygen and dissolved iron were controlled below 20 ppb and

⁽²⁾ The carbon steel was given as 1018 steel (UNS G10180). However, the carbon content is a bit beyond the range of 1018, as indicated in Table 1.

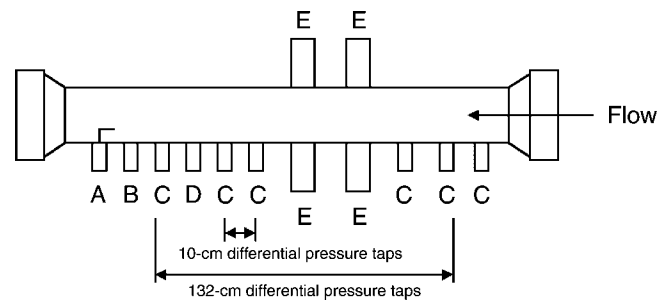


FIGURE 2. Test section of the high-pressure flow loop: (A) void fraction port; (B) thermocouple port; (C) differential pressure tap; (D) pH port; (E) corrosion probe insertion port.

TABLE 1
Chemical Composition of the Carbon Steel (wt%)

| C | Si | P | S | Mn | Al | Fe |
|------|------|------|------|------|------|---------|
| 0.21 | 0.38 | 0.09 | 0.05 | 0.05 | 0.01 | Balance |

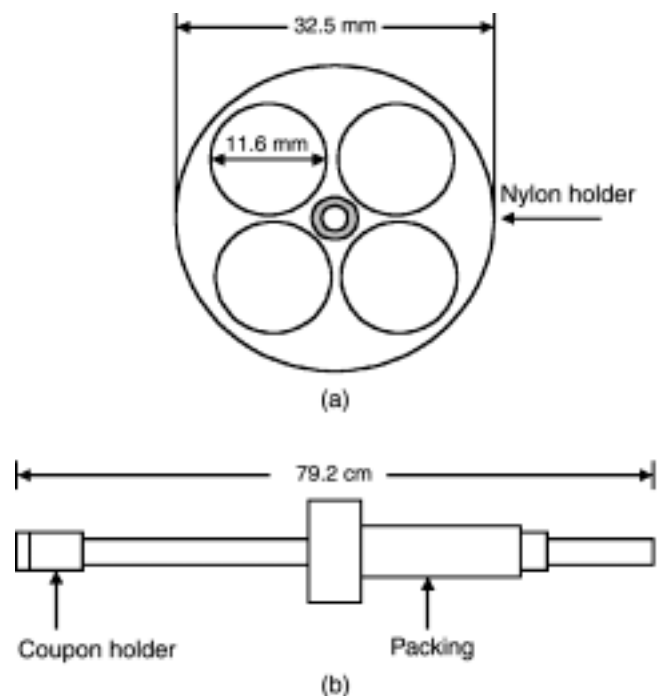


FIGURE 3. (a) Multiple coupon holder and (b) coupon holder probe.

10 ppm, respectively. The oxygen and iron levels were periodically monitored during testing.

At the start of the experiments, the ER probes and coupon holders were flush-mounted into the test section. The system was pressurized to the desired level and the liquid pump was turned on and adjusted to the required level. Finally, the recirculating gas pump was turned on to set the gas flow rate as required. For this work, the superficial liquid velocity (V_{sl}) of 0.05 m/s was used at superficial gas velocities

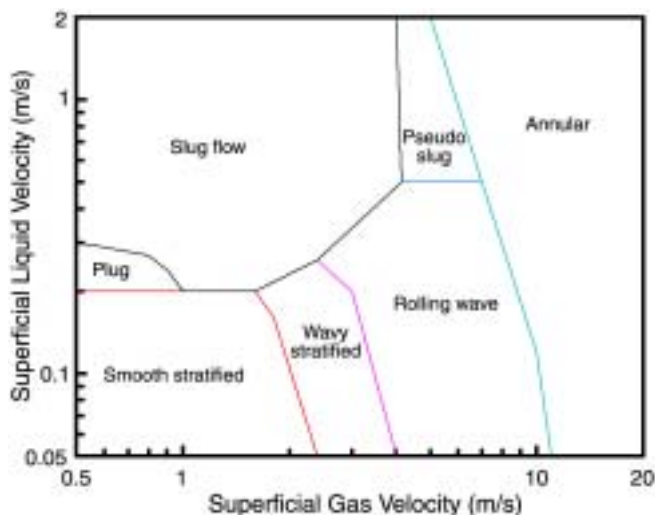


FIGURE 4. A typical flow regime map for gas/oil/water three-phase flow in horizontal pipes.¹⁸

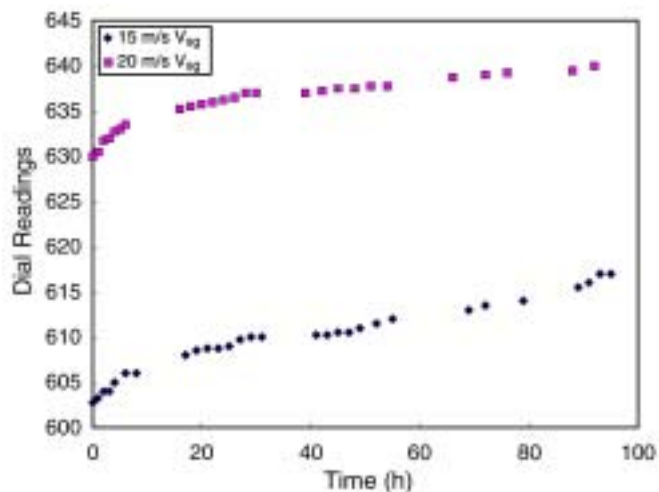


FIGURE 5. Change of dial readings with time at the top of the pipe for $V_{sl} = 0.05$ m/s, $T = 90^\circ\text{C}$, and $P = 0.45$ MPa.

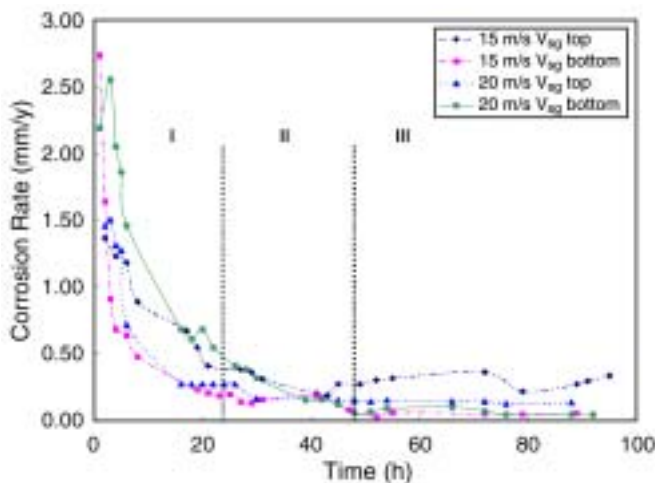


FIGURE 6. Change of corrosion rate with time at $V_{sl} = 0.05$ m/s, $T = 90^\circ\text{C}$, and $P = 0.45$ MPa.

(V_{sg}) of 15 m/s and 20 m/s at a pressure of 0.45 MPa and a temperature of 90°C . At these conditions, the flow regime is in annular flow according to the earlier work (Figure 4).¹⁸ The gas/liquid mixture enters the test section where the corrosion measurements are performed and is then returned to the storage tank where the mixture is separated. After separation, the gas is then fed to the recirculating pump.

ER probes were used with an automatic data logging system for recording the trend. At the same time, a manual corrosometer was used for checking the accuracy of the data. After 100 h, the liquid and gas pump were shut down and the system was depressurized gradually to 15 psig (0.2 MPa) within half an hour. The ER probes and the coupon holders were then removed from the test section. The coupons were rinsed with acetone immediately after removal from the test section. The pressure drops were re-

corded by the differential pressure transducer during each test. The average pressure drop in this work was ~ 60 Pa/m at a pH of ~ 5.0 .

RESULTS AND DISCUSSION

Corrosion Rate at Elevated Temperature Wet Gas Conditions

The raw data showing the time-dependent development of the dial readings of the manual corrosometer at V_{sg} of 15 m/s and 20 m/s are shown in Figure 5 for the top of the pipe. Different slopes developing in different time-dependent stages demonstrate the change of the corrosion rate with time. Based on this raw data, the change of corrosion rates can be plotted according to Figure 6.

Figure 6 shows the change of the corrosion rate with exposure time for both top and bottom of the pipe at 0.45 MPa, 90°C , and the V_{sl} of 0.05 m/s. It appears that for all test conditions the corrosion rates advanced in three stages that represent three different phases of the scale forming process. First, the corrosion rates decreased exponentially for ~ 25 h. This represents the corrosion product film formation process as previously suggested in the literature.^{6-7,10} It is known that elevated temperature favors the film formation and protective films form more easily, which consequently reduce the corrosion rate in the second stage.

The second stage was characterized by a rather slow further decrease of the corrosion rate up to ~ 50 h exposure time. As a result of the corrosion product film built-up in the first stage, a higher corrosion resistance of the steel was met by the barrier properties of the corrosion product scale. Consequently, smaller corrosion rates were observed within this time interval.

After ~50 h, the corrosion rates remained almost constant at a comparably low level of up to 0.5 mm/y at the beginning of the third stage. This indicates that the corrosion product films were very effective in preventing the corrosion progress.

The results obtained are in a good agreement with previous, yet unpublished, results.¹⁹ At elevated temperature (90°C) and pressure (2.1 MPa) in ASTM saltwater/hydrocarbon phase under full pipe flow, it was found that the corrosion product film became more compact after longer exposure times. After 10 h, the growth of the film tended to be stable. This implies a highly intensive scale growth with a decrease of the film porosity during the first 10 h of exposure and an equilibrium behavior afterward. It is reasonable that the stabilization process of the corrosion product film takes more time under annular flow conditions of this work with a highly increased flow intensity compared to the results of full pipe flow.

Figure 7 shows the average corrosion rates obtained from coupon weight-loss measurements for all test conditions applied. Three coupons were weighed after scale removal for each test. The columns represent the average value for each test condition while the error bars indicate the highest and lowest values among the three measurements. The results confirm the ER corrosion rate measurements (Figure 6), showing comparable corrosion rates at the bottom for 15 m/s V_{sg} and 20 m/s V_{sg} , and slightly increased values for the top of the pipe.

Surface Analysis

It can be noticed from both Figures 6 and 7 that for both test conditions the corrosion rate at the top is slightly increased compared to the bottom corrosion rate. This was caused by the different liquid film thickness and velocities in horizontal annular flow, which resulted in the growth of $FeCO_3$ scales with different scale properties on the top and bottom of the pipe. The effect of the flow intensity on the properties and morphology of the corrosion product scales formed under the conditions tested was investigated by surface analysis. Scanning electron microscopy (SEM) and metallurgical microscopy (MM) were applied to examine the surface morphology. The powerful structure and composition identification tools, x-ray diffraction (XRD) and x-ray photoelectron spectroscopy (XPS), were used to characterize the scale composition.

Visual examination of the ER probes and the test coupons after each test revealed that the surfaces were completely covered with dark-grey, almost black corrosion products. Only the bottom coupons, corroded at a superficial gas velocity of 15 m/s, showed uniformly distributed corrosion products. For the coupons at the bottom of the pipe, at 20 m/s V_{sg} , the surface topography exhibited characteristic plateaus of different heights. The top of the coupons for both

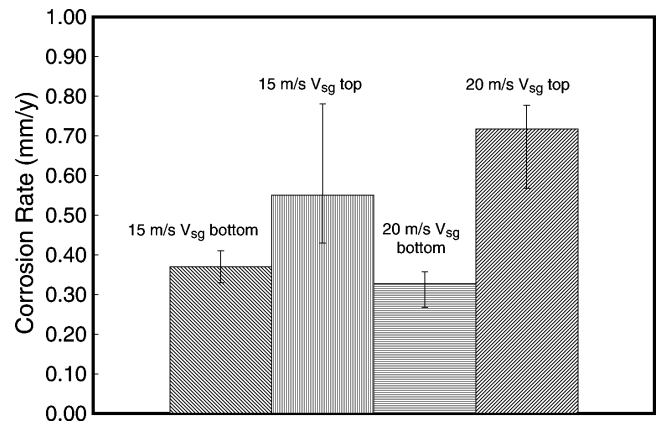


FIGURE 7. Average corrosion rate from coupon weight-loss measurement at $V_{sl} = 0.05$ m/s, $T = 90^\circ\text{C}$, and $P = 0.45$ MPa.

15 m/s and 20 m/s showed a nonuniform distribution of corrosion products.

SEM analysis was used for comparison purposes on all coupons, using the same magnification. Figure 8 shows the SEM images for the corrosion coupons at all test conditions, showing some common features among the coupons. The most common characteristic was the presence of crystals in all cases (white and light-gray-appearing areas in Figure 8). It was confirmed that $FeCO_3$ was the predominant product formed under the present test conditions by XRD and XPS analyses as shown below. It is reported in the literature¹² that $FeCO_3$ is stable and does not alter its structure with extended exposure to dry air when it is in the ripened form. Therefore, no further precautions were taken when removing the specimens from the flow loop after the tests.

Figures 8(a) and (b) show the SEM micrographs for the bottom and top coupons at 15 m/s V_{sg} . Compared with the crystals formed on the top coupon (~3 μm to 4 μm), a smaller average crystal size (~1 μm to 2 μm) can be observed at the bottom, yielding a more compact scale structure with decreased porosity. In horizontal annular flow with very low liquid content (0.05 m/s), the liquid film will always cover the bottom of the pipe while the top of the pipe may not get a continuous film all the time. In addition, the liquid film thickness at the bottom is increased compared to the top due to gravitational effects, resulting in a lower local film velocity at the bottom of the pipe. Consequently, a more uniform corrosion product film formation and growth at the pipe bottom is facilitated.

The effect of an enhanced gas velocity of 20 m/s on the scale morphology as shown in Figures 8(c) and (d) indicates that the topography of the $FeCO_3$ film formed on the top coupon becomes more uneven. The scale morphology at the bottom exhibits different plateaus. The raised areas patch together and show a higher porosity and increased surface

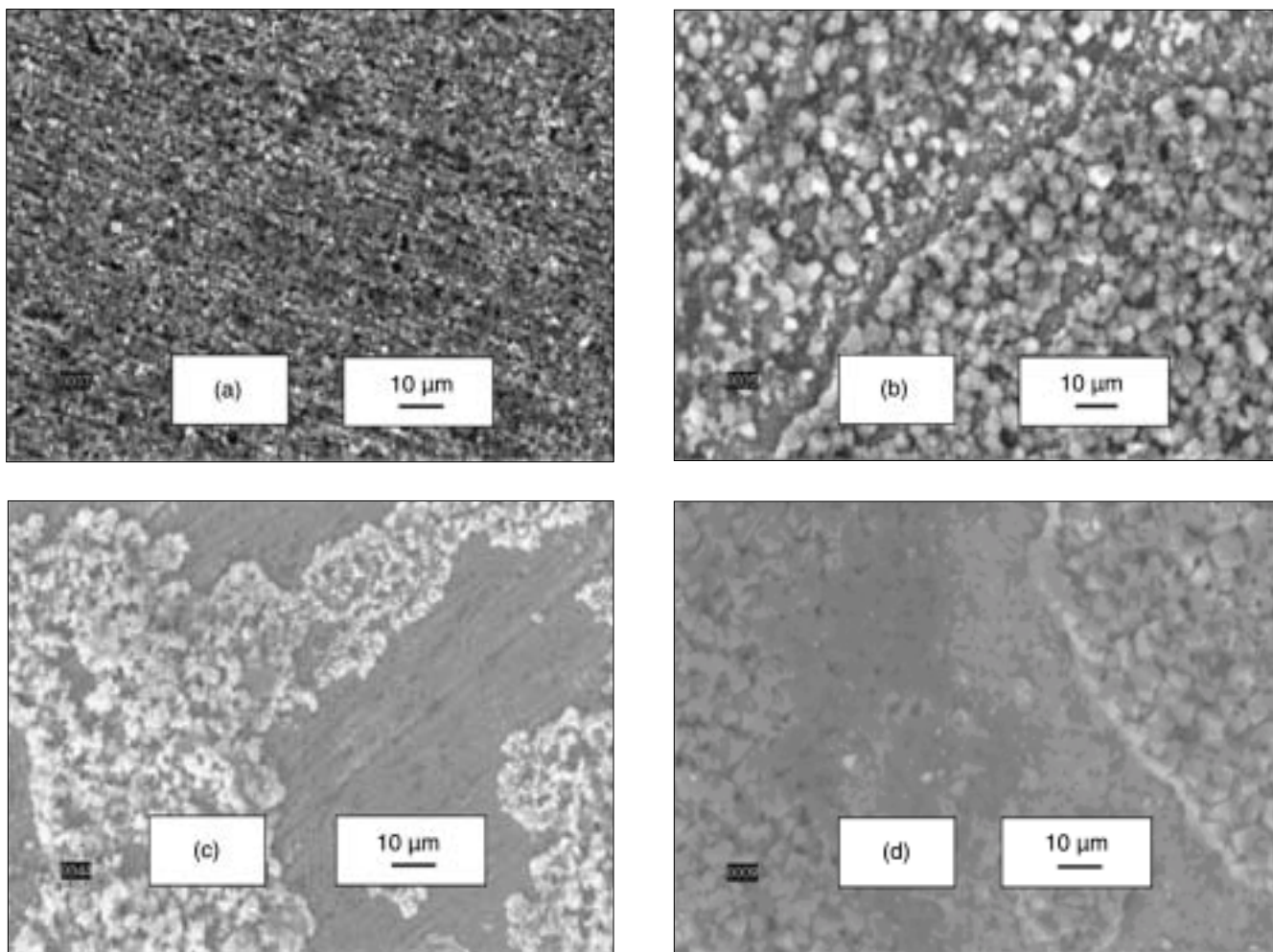


FIGURE 8. SEM micrographs for coupons at $V_{st} = 0.05$ m/s, $T = 90^\circ\text{C}$, and $P = 0.45$ MPa. (a) $V_{sg} = 15$ m/s bottom; (b) $V_{sg} = 15$ m/s top; (c) $V_{sg} = 20$ m/s bottom; (d) $V_{sg} = 20$ m/s top.

roughness. The lower plateaus are smoother and appear to be topotactically grown.

These results are in accordance with observations reported in the literature.^{1,8} At comparable temperatures, the scales formed in a CO_2 environment were usually thin (<30 μm), compact, and highly adherent, which was always related to a pronounced reduction of the corrosion rate.⁸ Once protective scales form at temperatures $\sim 80^\circ\text{C}$, they appear very robust and resistive even under severe flow conditions.¹

In Figures 9 through 11, the results of the surface analysis investigations are presented. Figure 9(a) shows the XRD spectrum for the top coupon corroded under 0.45 MPa CO_2 at 90°C , 20 m/s V_{sg} , and 0.05 m/s V_{st} . It shows both iron (Fe) and iron carbonate (FeCO_3) peaks at their corresponding characteristic Bragg's angles, 2θ . The high-intensity peaks for FeCO_3 appear at 2θ of 32.05, 52.87, 46.28, 24.77, 42.39, 38.42 degrees, which indicates that FeCO_3 is the corrosion product formed on the metal surface. The Fe peaks are the result of the penetration of the

x-ray into the metal substrate, which means the film is <30 μm in thickness, porous, or nonuniform.⁸ The bottom coupon's XRD spectrum (Figure 9 [b]) for the same test conditions revealed only the high-intensity iron peaks at 2θ of 44.6 and 65.2 degrees. The FeCO_3 peaks almost disappeared and remained at a very low level. This is because the film is much thinner and it presumably consists of some noncrystalline components. Further examination by XPS was applied on this coupon because XPS can provide element and chemical state identification for atoms located at the top atomic layers of the sample investigated.²⁰ Figure 10 shows Fe 2p, O 1s, and C 1s peaks in the XPS spectrum. The atomic ratio of Fe and O was found to be about 1:3, the carbon content was comparably high, most probably due to an insufficient removal of the hydrocarbon phase, resulting in some carbon contamination of the surface of the corrosion product scale.

The stability and therefore the protection of corrosion product scales strongly depends on their me-

chanical properties and on the scale thickness.¹³⁻¹⁴ Thin, compact scales exhibit much higher resistance against flow-induced corrosion attack than thick, porous scales. Figure 11 shows that the FeCO_3 scale thickness for both top and bottom is $<10\ \mu\text{m}$ for 15 m/s and 20 m/s V_{sg} , and in some areas, even as low as $\sim 1\ \mu\text{m}$. The scale exhibits a good adherence to the metal substrate and shows a low porosity, which are the preconditions for a high protectivity. No indications for the initiation of FILC were found for the test conditions investigated. Thus, the observed corrosion rates were low. A slightly higher degree of roughness at a V_{sg} of 20 m/s possibly increased the risk for the initiation of FILC at extended exposure times, which is intended to be confirmed by further experimental work.

CONCLUSIONS

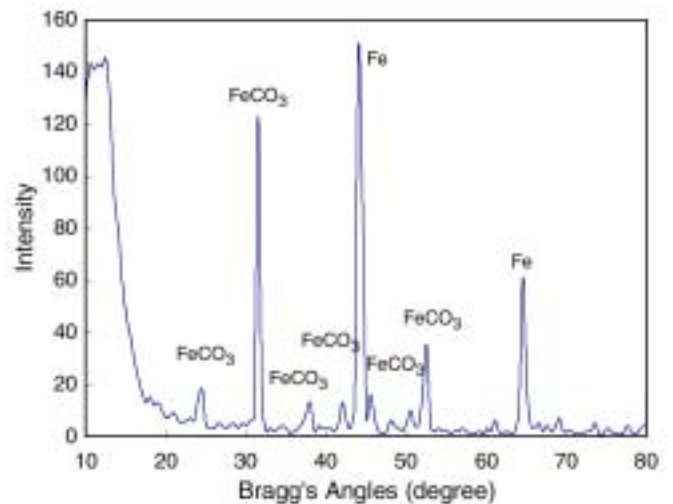
❖ In experiments with horizontal annular flow under wet gas CO_2 corrosion of plain carbon steel in a deionized water/hydrocarbon mixture (80:20 vol%) at V_{sg} of 15 m/s and 20 m/s and a V_{sl} of 0.05 m/s at 90°C , the average corrosion rate varied between 0.4 mm/y and 0.7 mm/y after 100 h exposure, dependent on the gas flow rate and on the position in the pipe. The general corrosion rates recorded by ER probes advanced in three stages, showing an exponential decay corresponding to the film forming process. The corrosion rate at the top of the pipe was slightly increased compared to the bottom of the pipe at horizontal wet gas flow as a result of the local difference of the liquid film thickness in horizontal annular flow regime, which resulted in the reduction of the protectivity of the FeCO_3 corrosion product scales formed at the top of the pipe. The formation of thin ($<10\ \mu\text{m}$), protective FeCO_3 layers was responsible for comparably low corrosion rates and protection from FILC, even at higher gas transportation capacities. The presence of a hydrocarbon phase exhibited a favorable effect even in non-inhibited, wet gas transportation systems, allowing acceptable gas flow rates when annular flow was maintained.

ACKNOWLEDGMENTS

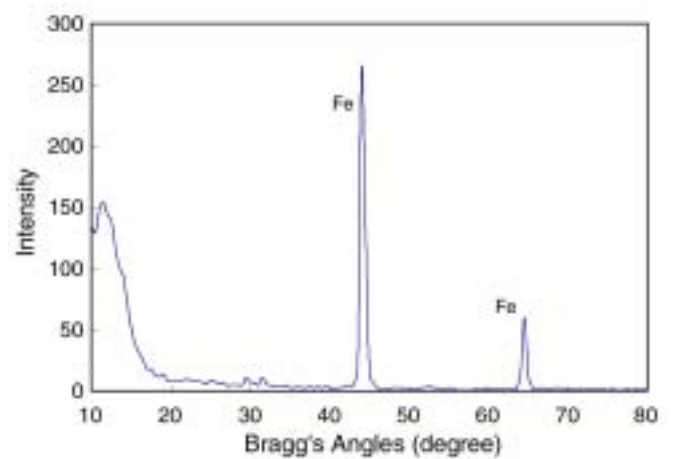
The authors acknowledge the Institute for Corrosion and Multiphase Technology at Ohio University and its member companies for the financial support of this research; M. Kordesch and D. Ingram in the Physics Department at Ohio University for helpful discussions about XRD analysis and XPS studies; and S. Nestic for helpful discussions.

REFERENCES

1. S. Olsen, A. Dugstad, "Corrosion under Dewing Conditions," CORROSION/91, paper no. 472 (Houston, TX: NACE International, 1991).



(a)



(b)

FIGURE 9 (a). XRD results for (a) top and (b) bottom of the pipe at $V_{\text{sl}} = 0.05\ \text{m/s}$, $V_{\text{sg}} = 20\ \text{m/s}$, $T = 90^\circ\text{C}$, and $P = 0.45\ \text{MPa}$.

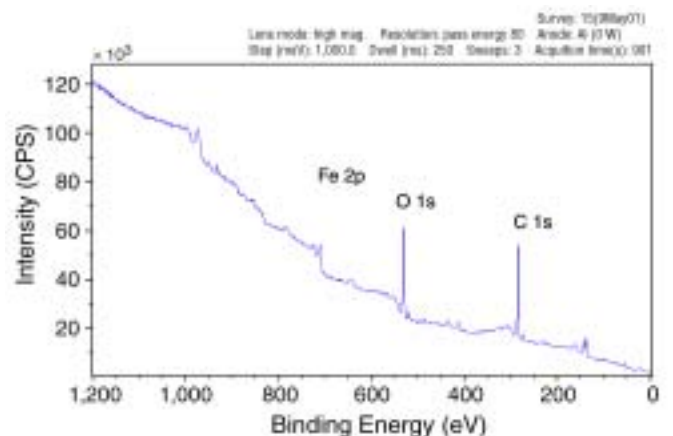


FIGURE 10. XPS spectrum for bottom coupons at $V_{\text{sl}} = 0.05\ \text{m/s}$, $V_{\text{sg}} = 20\ \text{m/s}$, $T = 90^\circ\text{C}$ and $P = 0.45\ \text{MPa}$.

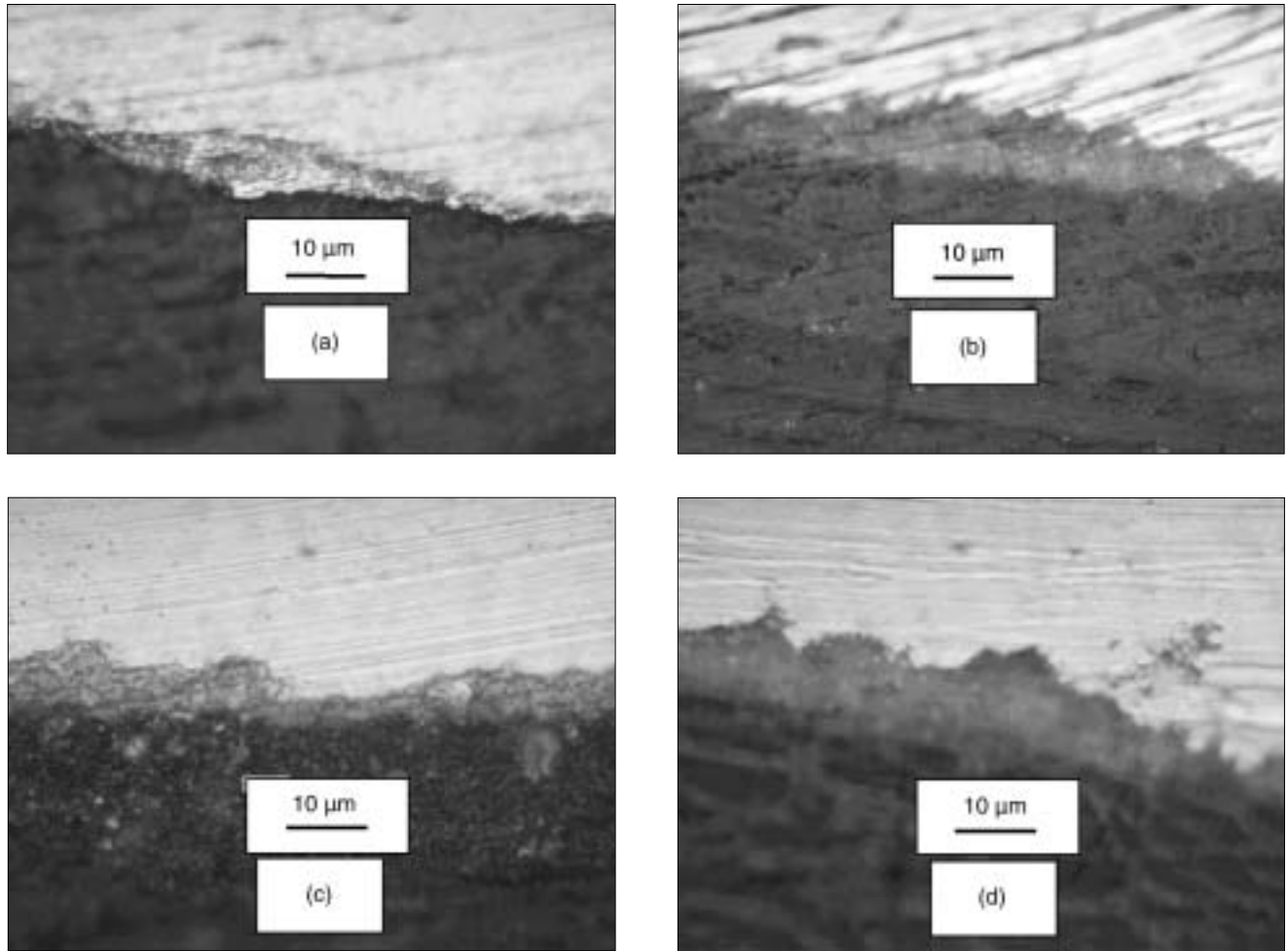


FIGURE 11. Cross sections for coupons at $V_{sl} = 0.05$ m/s, $T = 90^\circ\text{C}$, and $P = 0.45$ MPa. (a) $V_{sg} = 15$ m/s bottom; (b) $V_{sg} = 15$ m/s top; (c) $V_{sg} = 20$ m/s bottom; (d) $V_{sg} = 20$ m/s top.

2. M. Gopal, "Modeling Flow and Corrosion in Sweet Offshore Production," 23rd Annual Energy Source Technology Conference and Exhibition (ESTC and E), February 2000.
3. Y.M. Gunaltun, D. Supriyatman, J. Achmad, "Top-of-Line Corrosion in Multiphase Gas Lines, A Case History," CORROSION/99, paper no. 36 (Houston, TX: NACE, 1999).
4. Y.M. Gunaltun, D. Larrey, "Correlation of Cases of Top-of-Line Corrosion with Calculated Water Condensation Rates," CORROSION/2000, paper no. 71 (Houston, TX: NACE, 2000).
5. S.-L. Fu, M.J. Bluth, "Study of Sweet Corrosion under Flowing Brine and/or Hydrocarbon Conditions," CORROSION/94, paper no. 31 (Houston, TX: NACE, 1994).
6. A. Dugstad, "The Importance of FeCO_3 Supersaturation on the CO_2 Corrosion of Carbon Steels," CORROSION/92, paper no. 14 (Houston, TX: NACE, 1992).
7. S. Nešić, L. Lunde, Corrosion 50, 9 (1994): p. 717.
8. C.A. Palacios, J.R. Shadley, Corrosion 47, 2 (1991): p. 122.
9. A. Dugstad, L. Lunde, K. Videm, "Parametric Study of CO_2 Corrosion of Carbon Steel," CORROSION/94, paper no. 14 (Houston, TX: NACE, 1994).
10. F. de Moraes, J.R. Shadley, J. Chen, "Characterization of CO_2 Corrosion Product Scales Related to Environmental Conditions," CORROSION/2000, paper no. 30 (Houston, TX: NACE, 2000).
11. J.L. Crolet, N. Thevenot, S. Nešić, Corrosion 54, 3 (1998): p. 194.
12. J.K. Heuer, J.F. Stubbins, Corros. Sci. 41, 7 (1999).
13. G. Schmitt, M. Mueller, M. Papenfuss, "Understanding Localized CO_2 Corrosion of Carbon Steel from Physical Properties of Iron Carbonate Scales," CORROSION/99, paper no. 38 (Houston, TX: NACE, 1999).
14. G. Schmitt, T. Gudde, E. Strobel-Effertz, "Fracture Mechanical Properties of CO_2 Corrosion Product Scales and Their Relation to Localized Corrosion," CORROSION/96, paper no. 9 (Houston, TX: NACE, 1996).
15. G. Schmitt, C. Bosch, M. Mueller, "A Probabilistic Model for Flow-Induced Localized Corrosion," CORROSION/2000, paper no. 49 (Houston, TX: NACE, 2000).
16. G. Schmitt, C. Bosch, M. Mueller, "Modeling the Probability of Flow-Induced Localized Corrosion from Critical Hydrodynamic Data and Fracture Mechanics Data of Scales from CO_2 Corrosion of Steel," in Advances in Corrosion Control and Materials in Oil and Gas Production, European Federation of Corrosion Publication no. EFC 26 (London, U.K.: The Institute of Materials, 1999), Chapter 2, p. 24-51.
17. G. Schmitt, C. Bosch, P. Plagemann, "Wall Shear Stress Gradients in the Slug Flow Regime—Effects of Hydrocarbon and Corrosion Inhibitors," CORROSION/2002, paper no. 244 (Houston, TX: NACE, 2002).
18. A.-H. Lee, J.-Y. Sun, W.P. Jepson, "Study of Flow Regime Transitions of Oil-Water-Gas Mixtures in Horizontal Pipeline," Proc. 3rd Int. Offshore and Polar Eng. Conf., vol. 2 (Golden, CO: International Society of Offshore and Polar Engineers [ISOPE], 1993), p. 159-164.
19. T. Hong, "EIS Studies of Corrosion and Inhibition of Carbon Steel in Pipelines at High Temperature and High Pressure," presented at Institute of Corrosion and Multiphase Technology board meeting (1999).
20. G.C. Smith, Surface Analysis by Electron Spectroscopy (New York and London: Plenum Press, 1994), p. 5.